Available online at www.sciencedirect.com
ScienceDirect
Trans. Nonferrous Met. Soc. China 24(2014) 3118−3125
Transactions of Nonferrous Metals Society of China
www.tnmsc.cn

# Interfacial reactions between Ti-1100 alloy and CaO crucible during casting process

Bin-guo FU, Hong-wei WANG, Chun-ming ZOU, Pan MA, Zun-jie WEI

National Key Laboratory for Precision Heat Processing of Metal, Harbin Institute of Technology, Harbin 150001, China

Received 10 October 2013; accepted 10 February 2014

**Abstract:** Ti-1100 alloys were melted in a controlled atmospheric induction furnace equipped with a CaO crucible. The microstructure, chemical composition, microhardness and metal−crucible interfacial reactions were systematically investigated. The results demonstrate that the primary solidification microstructure in the as-cast alloys was the typical Widmanstätten structure. The interactions between crucible and molten alloys are attributed to slight chemical dissolution and weak physical erosion. According to the line scanning analysis, the interfacial layer ($\alpha$-case) thicknesses of Ti-1100 samples in the bottom and side wall are about 18 and 17 μm, respectively, which are slightly lower than those presented from microhardness tests (25 and 20 μm). The formation of $\alpha$-case was caused by interstitial oxygen atoms. The standard Gibbs energy of reaction CaO(s)=Ca+O for Ti-1100 alloy was also determined. The equilibrium constant and the interaction parameter between calcium and oxygen were obtained as lg $K$=−3.14 and $e_{\mathrm{O}}^{\mathrm{Ca}}$ =−3.54.
**Key words:** Ti-1100 alloy; CaO crucible; interfacial reaction; casting; microstructure

## 1 Introduction

Ti-1100 alloy, as a near-$\alpha$ high temperature titanium alloy designed by Timet, USA in 1988 for elevated temperature applications up to 600 °C, is developed for compressor disks and blades which are subjected to high temperatures complicated loading [1−3]. To date, the fabrication technologies mainly focus on wrought and power metallurgy processes. However, the former is quite prone to chemical and microstructure heterogeneity while the latter is limited by the freedom of size and shape, which makes the production costs extremely expensive [4]. Therefore, casting is a feasible and effective method to solve the above problems.

A significant amount of superheating is necessary for avoiding misrun and cold laps due to low fluidity of high temperature titanium alloys at pouring temperatures [5,6]. Vacuum arc remelting (VAR) and induction skull melting (ISM) were employed to melt previous produced billets and scrap; however, it is difficult to control the melting composition and superheating [7]. The usage of a ceramic crucible (such as $Al_2O_3$ [8], $ZrO_2$ [9,10], $Y_2O_3$ [11] and CaO [12] crucible) induction melting process by traditional melting stocks, is a possible solution, which can decrease production costs and eliminate partial casting defects, such as misrun. During casting process of titanium alloys, the surface reaction layer called '$\alpha$-case' occurs due to the high reactivity of the molten alloys with refractory materials. It is difficult to machine the $\alpha$-case and the $\alpha$-case can induce crack initiation and propagation [13,14]. Noticeably, the $\alpha$-case layers can be eliminated during the chemical milling process [13].

To the best of our knowledge, no refractory materials have been developed so far which are completely resistant to molten titanium alloys. What's more, interactions between metal and crucible materials are possible to occur during the melting stage, leading to the metal contamination. According to the thermodynamic calculations by KOSTOV and FRIEDRICH [15], only a few oxide-based ceramics exhibit sufficient thermochemical stability above the melting temperature of titanium, including CaO, $ZrO_2$, and $Y_2O_3$. However, disadvantages to use $ZrO_2$ crucibles for melting titanium alloys are low thermal conductivity, high thermal expansion, and lack of stability in the structure, which results in decreased resistance to thermal shock. The drawbacks of $Y_2O_3$ crucibles are their low thermal shock resistance and high cost. Compared with the free Gibbs energy of formation, CaO has a very

**Foundation item:** Projects (51001041, 51171054) supported by the National Natural Science Foundation of China
**Corresponding author:** Zun-jie WEI; Tel: +86-451-86418740; Fax: +86-451-86418131; E-mail: weizj@hit.edu.cn
DOI: 10.1016/S1003-6326(14)63450-6

low negative value which is only inferior to $Y_2O_3$, indicating that it is a good choice to produce melting crucibles for titanium alloys [16,17]. Although some researchers have focused their studies on the CaO refractories to develop a crucible material for melting Ti−Al based alloys [18,19], using CaO crucible to melt high temperature titanium alloys had not been reported. As a multi-component alloy, the interfacial reactions and the $\alpha$-case formation mechanism between the melt and CaO crucible may be different from that of Ti−Al alloys. Some literatures defined the thickness of the $\alpha$-case layers by surface microhardness test during casting process of titanium alloys [19,20]; however, such method is inaccurate to detect the thickness of the interfacial layer, especially for the thin reaction layer. In order to clearly reveal the thickness of $\alpha$-case layer, the distribution of the elements in the $\alpha$-case region and its chemical composition should be clarified firstly.

The purpose of this work is to investigate the alloy contamination by the microstructure, composition and surface microhardness of the alloy solidified inside the crucible. The characteristics of $\alpha$-case layers were revealed by line scanning and microhardness test. The compatibility between the Ti-1100 alloy melt and the CaO crucible was also investigated.

## 2 Experimental

Ti-1100 alloy (Ti−6Al−2.7Sn−0.4Mo−4.0Zr−0.45Si; mass fraction, %) was selected for the experimental material, which was prepared from sponge titanium (99.8%), high purity aluminum (99.99%), pure tin (99.9%), sponge zirconium (99.4%), pure molybdenum (99.95%) and pure silicon (99.5%). In order to improve the efficiency of melting and reduce the evaporation, the above mentioned materials were compressed into blocks by a press machine before the melting process. Melting stocks weighing 4 kg were melted in an induction melting furnace equipped with a commercial CaO crucible, under a dry high purity argon (99.999%) atmosphere at 1000 Pa. Before heating, the chamber was evacuated up to $10^{-2}$ Pa and backfilled with argon 3 times in order to reduce the oxygen content to a minimum level. After the raw materials were completely melted, temperature measurements were carried out by the type C (W−5Re/W−26Re) immersion thermocouple with a Mo−$Al_2O_3$ protection and the melt was held at 1973 K for 2 min. Finally, the alloy melt was poured into a graphite mould and the solidified sample had a thickness of 12 mm, then the remaining melt was solidified and cooled to room temperature inside the crucible to simulate the worst practical situation concerning the occurrence of a metal-refractory interaction, as shown in Fig. 1.


**Fig. 1** Photographs of sample solidified inside CaO crucible: (a) Top view; (b) Side view

An Olympus optical microscope (OM) and scanning electron microscope (SEM) (FEI, QUANTA 200F) equipped with an energy dispersive spectroscope (EDS) were used to characterize the microstructures, chemical composition and quantitative elements distribution of the reaction layer of titanium castings. Overall oxygen content was measured by the ONH836 oxygen, nitrogen and hydrogen determinator using the inert gas fusion technique. The dimensions of the test specimen were $d5\times6$ mm. In order to ensure reproducibility, three samples were tested. Microhardness was evaluated on a Huayin hardness tester with 0.98 N load for 10 s and 10 μm intervals. More than ten indentations were performed on each position to obtain the mean value.

## 3 Results and discussion

### 3.1 Microstructure

The microstructures of the Ti-1100 alloy poured into the graphite mould and solidified inside the CaO crucible are both Widmanstätten structure with basket weave features as shown in Fig. 2. It shows a typical lamellar structure of (near-$\alpha$) titanium alloys where individual $\alpha$-laths are separated by a thin layer of retained prior $\beta$ phase. The prior $\beta$ grain size and $\alpha$-laths

spacing calculated by a mean linear intercept method in Figs. 2 (a) and (b) are approximately 320 μm, 8.1 μm and 600 μm, 15.7 μm, respectively. The values of the sample solidified inside the crucible are much larger than those solidified in the graphite mould, due to the lower cooling rate.

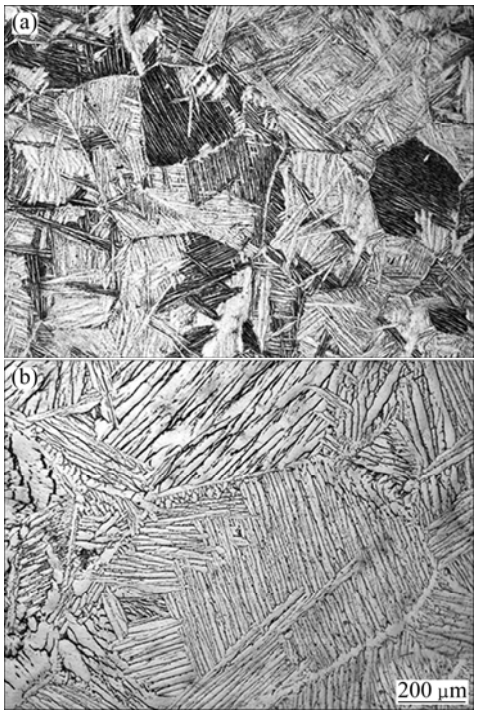


**Fig. 2** OM microstructures of Ti-1100 samples solidified in graphite mould (a) and inside CaO crucible (b)

No small CaO particles can be found in both the Ti-1100 samples solidified in the graphite mould and inside the CaO crucible from Fig. 3. Table 1 presents the chemical compositions of spots A and B marked in Fig. 3. Although elements vaporization (such as aluminum and tin) may occur [16], no obvious elements loss of the alloy was detected. At the beginning of the melting process, the elements with low melting temperatures kept a soft stage (mushy zone), and then they immediately dissolved in Ti with increasing of output power. Besides, electromagnetic stirring is conducive to make the composition homogeneous [21,22]. From Table 1, it is also revealed that each sample has a weak contamination of Ca dissolved into the matrix. The presence of Ca in solution reveals that some sort of interaction occurred between the CaO crucible and the cast alloy. In addition, the Ca content in the sample solidified inside the crucible is apparently higher than that solidified in the graphite mould, due to the long reaction time. The oxygen content of sample solidified inside the crucible ($\sim 730\times10^{-6}$) is lower than the calcium content ($\sim 1500\times10^{-6}$). The final Ca and oxygen contents of the ingot are different due to the different vapour pressures of the elements during VIM process [23].

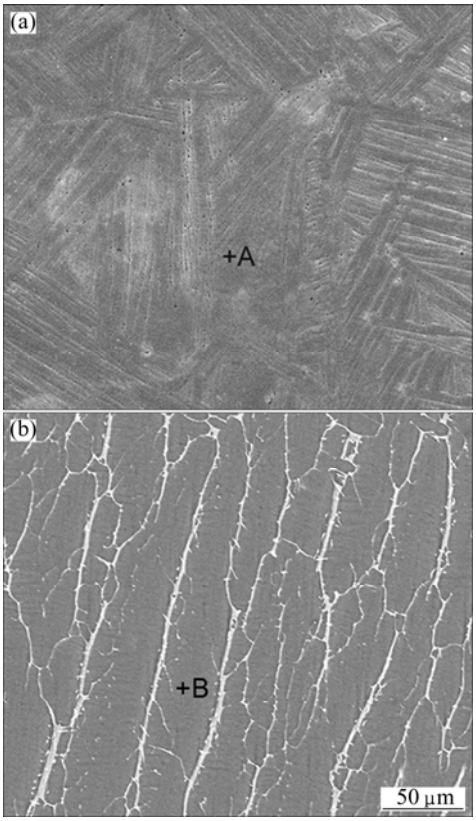


**Fig. 3** SEM microstructures of Ti-1100 samples solidified in graphite mould (a) and inside CaO crucible (b)

**Table 1** Compositions of spots A and B marked in Fig. 3

| Spot | *w*/% | | | | | | |
|---|---|---|---|---|---|---|---|
| | Al | Si | Zr | Mo | Sn | Ca | Ti |
| A | 6.79 | 0.50 | 4.38 | 0.48 | 2.90 | 0.08 | 84.87 |
| B | 6.35 | 0.54 | 4.45 | 0.45 | 3.17 | 0.15 | 84.89 |

### 3.2 Metal−crucible interface

Figure 4 shows the surface microstructures of Ti-1100 sample solidified inside the CaO crucible in different interfacial regions. It is obvious to see that there are distinct *α*-case reaction layers at the interface. Generally, the *α*-case is known to be developed by interstitials during casting process, such as carbon, nitrogen, and especially the oxygen dissolved from metal oxide crucible materials [4,13].

During the molten Ti (around 2000 K) solidifying inside the CaO crucible, the reaction of *α*-case between Ti and interstitial oxygen can be described as follows [13,24]:

$$\mathrm{Ti(l)+O_2(g)=TiO_2(s),}\ \Delta G^{\Theta}_{\mathrm{TiO_2}}=-585.83\ \mathrm{kJ/mol} \quad (1)$$

$$\mathrm{Ti(l)+1/2O_2(g)=TiO(s),}\ \Delta G^{\Theta}_{\mathrm{TiO}}=-356.30\ \mathrm{kJ/mol} \quad (2)$$

$$\mathrm{Ca(l)+1/2O_2(g)=CaO(s),}\ \Delta G^{\Theta}_{\mathrm{CaO}}=-401.71\ \mathrm{kJ/mol} \quad (3)$$

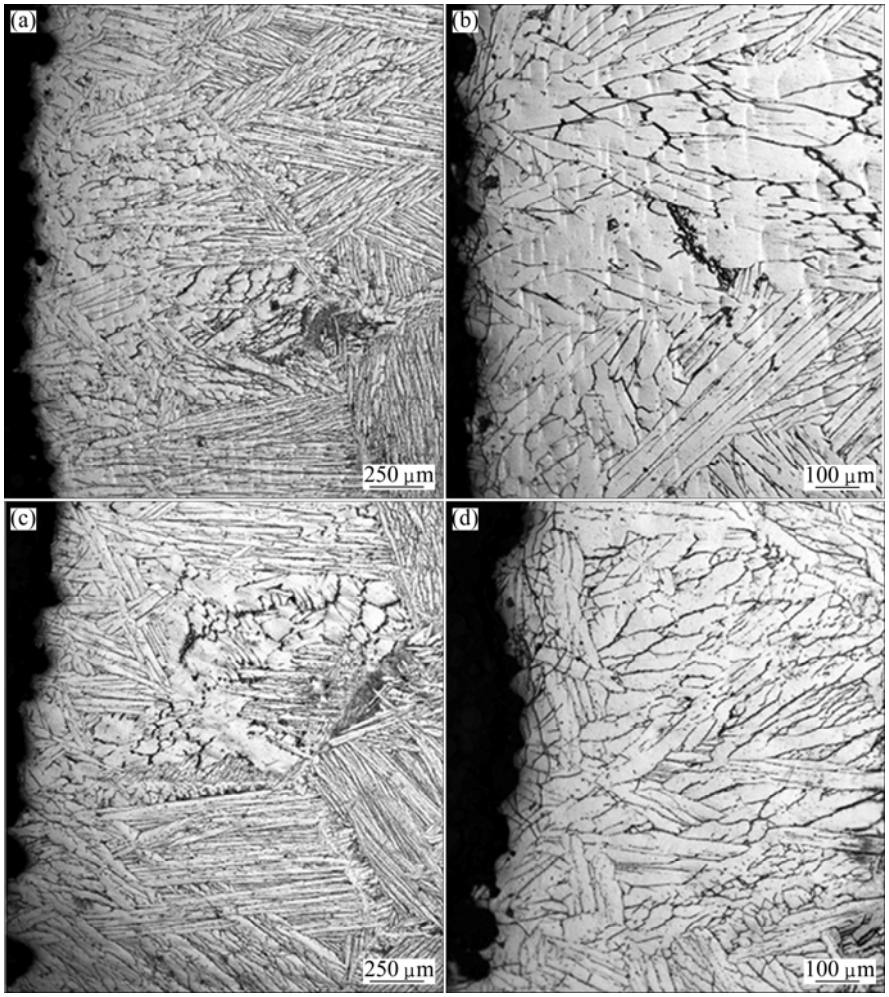


**Fig. 4** Microstructures of metal−crucible interfacial regions of as-cast Ti-1100 samples: (a), (b) Bottom; (c), (d) Side wall

$$\mathrm{Ti(l)} + 2\mathrm{CaO(s)} = \mathrm{TiO_2(s)} + \mathrm{Ca(l)},$$

$$\Delta G^{\Theta} = 217.60\ \mathrm{kJ/mol} \quad (4)$$

$$\mathrm{Ti(l)+CaO(s)=TiO(s)+Ca(l)}\ ,\quad \Delta G^{\Theta} = 45.41\ \mathrm{kJ/mol} \quad (5)$$

According to Eqs. (4) and (5), the formation of the $\alpha$-case induced by interstitial oxygen cannot occur spontaneously. Therefore, the chemical reaction between the molten Ti and the ceramic crucible could not be explained by the conventional $\alpha$-case formation mechanism.

The results of Vickers microhardness with different distances from the sample surface are shown in Fig. 5. With increasing the distance from the sample surface to its interior, the microhardness of the samples solidified inside the CaO crucible decreases drastically and then is stable at about 40 μm. The distances are around 25 μm and 20 μm in the bottom and the side wall, respectively, corresponding to the $\alpha$-case extension. Further increasing the distances from the surface to the bulk, the microhardness kept a nearly constant value (HV424 for side wall and HV437 for bottom). The samples in the bottom show a slightly higher microhardness than those in the side wall, and there are no overlaps between the two curves. However, as for the samples poured into the graphite moulds, the microhardness of bulk samples is located at a constant value around HV410 without microhardness gradients.

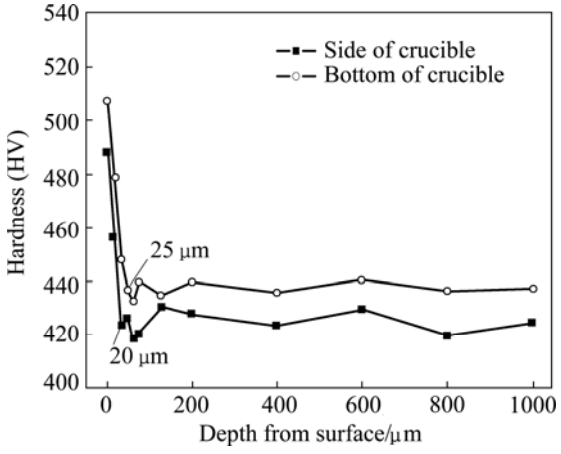


**Fig. 5** Hardness profiles in interfacial regions of as-cast Ti-1100 samples solidified inside CaO crucible

To further investigate the interfacial reaction between the metal and the CaO crucible, the solute distribution of the $\alpha$-case was detected by line scanning, as shown in Fig. 6 and Fig. 7. The $\alpha$-case layer comprises a reaction layer (A) and a harder layer (B). Layer A can be distinguished from back-scattered electron (BSE) images for the phases on the alloy surface are different from those in the matrix and layer B. The reactive diffusion characteristics of the element between titanium alloys and CaO crucible can be drawn clearly by line scanning. It is found that the thickness of the $\alpha$-case layer of the Ti-1100 alloy is approximately 18 μm in the bottom interfacial region, including the reaction layer (A) with a thickness of about 11 μm and the harder layer (B) with an approximate thickness of 7 μm.

Figure 7 shows the thickness of the $\alpha$-case layer in the side wall interfacial region for Ti-1100 samples solidified inside the CaO crucible, which is approximately 17 μm comprising an A layer with a constant thickness of 6 μm and a B layer with a constant thickness of 11 μm. By comparing Fig. 6 with Fig. 7, the thicknesses of the two layers are nearly the same. However, the depth of the bottom reaction layer is much thicker than that of the side wall. It can also be observed

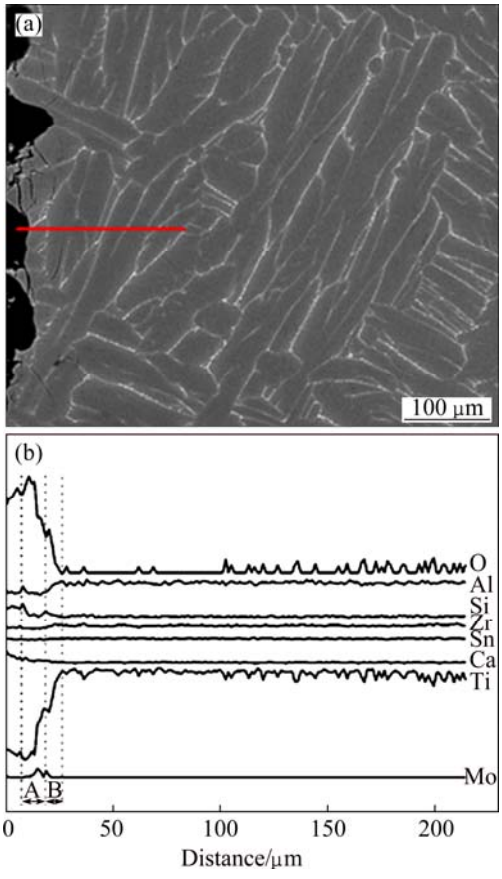


**Fig. 6** SEM image (a) and elemental distribution curves (b) in bottom interfacial region between Ti-1100 sample and CaO crucible

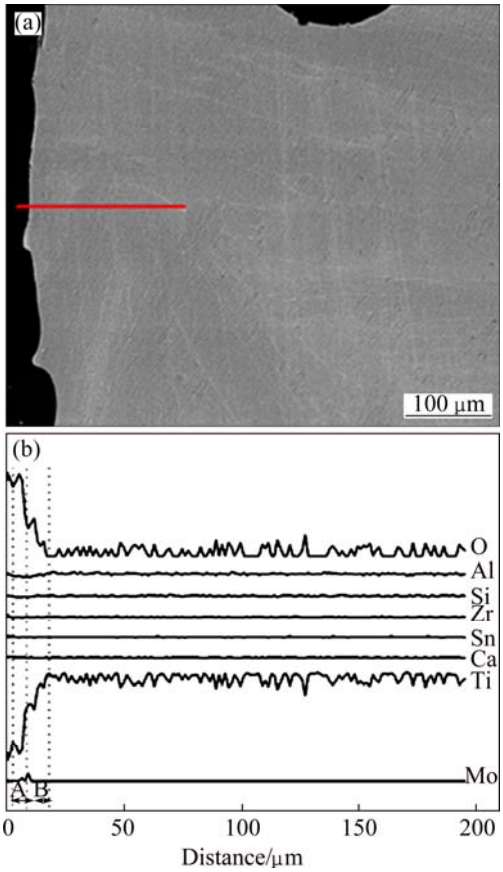


**Fig. 7** SEM image (a) and elemental distribution curves (b) in side wall interfacial region between Ti-1100 sample and CaO crucible

that the Ti and O elements exhibit a similar diffusion regular pattern in the $\alpha$-case layer. The content of Ti element increases with the increase of depth from the surface to the inner of the samples whereas the content of O element decreases. The contents of Ca, Al, Si and Zr in the samples solidified inside the bottom crucible have a few of changes, while there are no obvious changes in the side wall from the outer layer to the inner layer. This is attributed to the stirring effect of induction heating with the intermediate frequency of the melting furnace (2.75 kHz). According to the following equation, the electromagnetic stirring force can reach $4.8\times10^3$ N/m$^2$:

$$F = 31600P_2 / S \cdot \sqrt{1/\rho_2 f} \quad (6)$$

where $F$ is the electromagnetic stirring force; $P_2$ is the sensor output power; $\rho_2$ is the electrical resistivity of molten metal; $f$ is the frequency; $S$ is the surface area of the metal surrounded by the sensor.

The oxygen contents of samples solidified inside the crucible and in the graphite mould are ~$730\times10^{-6}$ and ~$625\times10^{-6}$, respectively, which are lower than the results reported by GOMES et al [16] and LIU et al [25] for TiAl alloys obtained in CaO crucibles as well as in other ceramic crucibles [5,7]. The results reveal that it is

feasible to use CaO crucible to melt high temperature titanium alloys if the interaction mechanism ($\alpha$-case extension) between the crucible and the molten alloy is determined.

As mentioned above, there is no chemical reaction occurring between the cast alloy and CaO crucible due to higher stability of CaO than $TiO_2$ and other metal oxides. However, the presence of Ca and O in the samples clearly reveals that the reactions between crucible and melts occurred. Combined with the previous published results, a possible reason for the alloy contamination is due to the dissolution of the ceramic crucible by the molten alloy [26−30]. Thus, physical erosion and solution effects need to be taken into consideration to obtain a more realistic picture. Figure 8 shows that the inner surfaces of crucible are considerably infiltrated by the melt while the original shape of the crucible is maintained. This suggested that except for the mechanical infiltration of the ceramic, no significant chemical reaction occurred. The slight dissolution of the CaO crucible can be confirmed from the enrichment of calcium and oxygen in the surface layer of the as-cast samples (Table 1, Figs. 6 and 7).

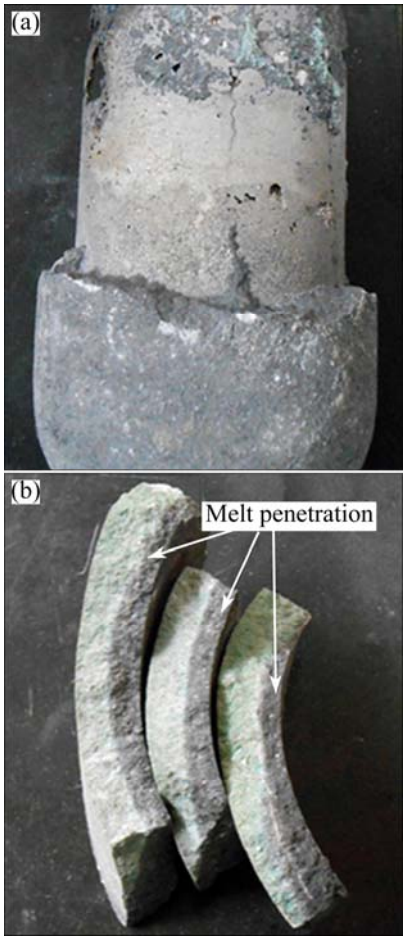


**Fig. 8** Photographs of CaO crucible after melting phase separation between metal and CaO (a), cross-section of infiltrated CaO crucible (b)

Previous investigations revealed [16,31−33] that the microhardness can be considered an index of contamination (such as interstitial oxygen) which resulted from metal−mould reaction during the process of casting. In this case, although the oxygen concentration is low and the composition analysis is insensitive, the microhardness profile can still be drawn as an evidence of the distribution of oxygen. Hence, based on the microstructure, microhardness profile and line scanning measurements, we conclude that the formation of the $\alpha$-case is caused by interstitial oxygen atoms.

The reaction between solid CaO and molten Ti alloy and its equilibrium constant $K$, are expressed by Eqs. (7) and (8).

$$\mathrm{CaO(s)=Ca+O} \tag{7}$$

$$K=\frac{f_{\mathrm{Ca}}\cdot w(\mathrm{Ca})\cdot f_{\mathrm{O}}\cdot w(\mathrm{O})}{a_{\mathrm{CaO}}} \tag{8}$$

where $a_{\mathrm{CaO}}$ is the activity of CaO relatively to pure solid CaO; $f_{\mathrm{Ca}}$ and $f_{\mathrm{O}}$ are the activity coefficients of calcium and oxygen relatively to 1% mass fraction; $w$(Ca) and $w$(O) are calcium and oxygen mass fraction of the molten Ti-1100 alloy respectively. Sine a CaO crucible is used, $a_{\mathrm{CaO}}$ is the unity. Therefore, Eq. (9) can be obtained by taking logarithms of both sides of Eq. (8).

$$\lg K=\lg f_{\mathrm{Ca}}+\lg f_{\mathrm{O}}+\lg[w(\mathrm{Ca})\cdot w(\mathrm{O})] \tag{9}$$

The activity coefficients of calcium and oxygen, $f_{\mathrm{Ca}}$ and $f_{\mathrm{O}}$, are expressed as Eqs. (10) and (11), respectively, by using the first-order interaction parameters.

$$\lg f_{\mathrm{Ca}}=e_{\mathrm{Ca}}^{\mathrm{Ca}}w(\mathrm{Ca})+e_{\mathrm{Ca}}^{\mathrm{O}}w(\mathrm{O}) \tag{10}$$

$$\lg f_{\mathrm{O}}=e_{\mathrm{O}}^{\mathrm{Ca}}w(\mathrm{Ca})+e_{\mathrm{O}}^{\mathrm{O}}w(\mathrm{O}) \tag{11}$$

We assumed that the self-interaction coefficients, $e_{\mathrm{Ca}}^{\mathrm{Ca}}$ and $e_{\mathrm{O}}^{\mathrm{O}}$, can be ignored since the oxygen and calcium contents are very small in the melts. Thus, Eq. (12) can be obtained from Eqs. (9), (10) and (11):

$$\lg K=e_{\mathrm{Ca}}^{\mathrm{O}}w(\mathrm{O})+e_{\mathrm{O}}^{\mathrm{Ca}}w(\mathrm{Ca})+\lg[w(\mathrm{Ca})\cdot w(\mathrm{O})] \tag{12}$$

$$e_{\mathrm{Ca}}^{\mathrm{O}}=(M_{\mathrm{r,Ca}}/M_{\mathrm{r,O}})e_{\mathrm{O}}^{\mathrm{Ca}}=2.505e_{\mathrm{O}}^{\mathrm{Ca}} \tag{13}$$

where $M_{\mathrm{r,Ca}}$ and $M_{\mathrm{r,O}}$ are the relative molecular masses of calcium and oxygen, respectively. So, Eq. (14) can be deduced from Eqs. (12) and (13).

$$\lg[w(\mathrm{Ca})\cdot w(\mathrm{O})]=\lg K-e_{\mathrm{O}}^{\mathrm{Ca}}[w(\mathrm{Ca})+2.505w(\mathrm{O})] \tag{14}$$

Therefore, lg[$w$(Ca)·$w$(O)] is shown to have a linear relationship with [$w$(Ca)+2.505$w$(O)]. $K$ (equilibrium constant) and $e_{\mathrm{O}}^{\mathrm{Ca}}$ were obtained from the experiment results (calcium and oxygen contents in cast alloys) and Eq. (14). The values of lg $K$ and $e_{\mathrm{O}}^{\mathrm{Ca}}$ were −3.14 and −3.54 at 1973 K, respectively. The Gibbs free energy of

reaction (Eq. (7)) is 118599.4 J/mol.

## 4 Conclusions

1) The primary solidification microstructure in the as-cast alloys reveals the Widmanstätten structure with basket weave features. The prior $\beta$ grain sizes and $\alpha$-laths spacings of Ti-1100 alloy poured into the graphite mould and solidified inside the CaO crucible are approximately 320 μm, 8.1 μm and 600 μm, 15.7 μm, respectively.

2) The interaction between molten alloys and CaO crucible directly influenced the chemical composition and microhardness of the alloys. The oxygen content and microhardness in the interfacial regions are higher than those in the interior.

3) The formation of the $\alpha$-case can be attributed to the interstitial oxygen that dissolved from crucible materials, and the interfacial layer ($\alpha$-case) thicknesses of Ti-1100 samples in the bottom and side wall are about 18 and 17 μm, respectively.

4) For equilibrating molten Ti-1100 alloy with solid CaO at 1973 K, the standard Gibbs energy of reaction CaO(s)=Ca+O was determined to be 118599.4 J/mol. The equilibrium constant and the interaction parameter between calcium and oxygen were obtained as lg $K$=−3.14 and $e_{\mathrm{O}}^{\mathrm{Ca}} = -3.54$.

## References


[1] CUI W F, LIU C M, ZHOU L, LUO G Z. Characteristics of microstructures and second-phase particles in Y-bearing Ti-1100 alloy [J]. Mater Sci Eng A, 2002, 323: 192−197.

[2] LEE D H, NAM S W. High temperature fatigue behavior in tensile hold LCF of near-alpha Ti-1100 with lamellar structure [J]. J Mater Sci, 1999, 34: 2843−2849.

[3] LEE D H, NAM S W, CHOE S J. Effect of $\alpha$ lamellae width on creep-fatigue behavior in near-$\alpha$ Ti-1100 with lamellar structure [J]. Scripta Mater, 1999, 40: 265−270.

[4] SUNG S Y, KIM Y J. Influence of Al contents on alpha-case formation of Ti−$x$Al alloys [J]. J Alloys Compd, 2006, 415: 93−98.

[5] BARBOSA J, RIBEIRO C S, MONTEIRO A C. Influence of superheating on casting of $\gamma$-TiAl [J]. Intermetallics, 2007, 15: 945−955.

[6] MI J, HARDING R A, WICKINS M, CAMPELL J. Entrained oxide films in Ti−Al castings [J]. Intermetallics, 2003, 11: 377−385.

[7] KUANG J P, HARDING R A, CAMPBELL J. Investigation into refractories as crucible and mould materials for melting and casting $\gamma$-TiAl alloys [J]. Mater Sci and Technol, 2000, 16: 1007−1016.

[8] DLOUHÝ A, DOČEKALOVÁ K, ZEMČÍK L. Vacuum induction melting and investment casting technologies tailored to near-gamma TiAl alloys [J]. Mater Sci Forum, 2007, 539−543: 1463−1468.

[9] BARBOSA J, RIBEIRO C S. Influence of crucible material on the level of contamination in TiAl using induction melting [J]. Int J Cast Met Res, 2000, 12: 293−301.

[10] CHEN Yan-fei, XIAO Shu-long, TIAN Jing, XU Li-juan, CHEN Yu-yong. Effect of particle size distribution on properties of zirconia ceramic mould for TiAl investment casting [J]. Transactions of Nonferrous Metals Society of China, 2011, 21: s342−s347.

[11] HOLCOMBE C E, SERANDOS T R. Consideration of yttria for vacuum induction melting of titanium [J]. Metall Trans B, 1983, 14: 497−499.

[12] SUN TT, JIANG M, LI C H, LU X G, LIU W D. Modification of CaO refractory for melting titanium alloys and its hydration resistance [J]. Adv Mater Res, 2001, 177: 502−505.

[13] SUNG S Y, KIM Y J. Alpha-case formation mechanism on titanium investment castings [J]. Mater Sci Eng A, 2005, 405: 173−177.

[14] CRUZ R V B, SAYEG I J, MUTARELLI P S, PINEDO C E. Effect of the ceramic mould composition on the surface quality of as-cast titanium alloy [J]. J Mater Sci, 2005, 40: 6041−6043.

[15] KOSTOV A, FRIEDRICH B. Predicting thermodynamic stability of crucible oxides in molten titanium and titanium alloys [J]. Comput Mater Sci, 2006, 38: 374−385.

[16] GOMES F, BARBOSA J, RIBEIRO C S. Induction melting of $\gamma$-TiAl in CaO crucibles [J]. Intermetallics, 2008, 16: 1292−1297.

[17] CUI Ren-jie, TANG Xiao-xia, GAO Ming, ZHANG Hu, GONG Sheng-kai. Thermodynamic analysis of interactions between Ti−Al alloys and oxide ceramics [J]. Transactions of Nonferrous Metals Society of China, 2012, 22: 887−894

[18] WANG Li-gang, ZHENG Li-jing, CUI Ren-jie, YANG Li-li, ZHANG Hu. Microstructure and mechanical properties of cast Ti−47Al−2Cr−2Nb alloy melted in various crucibles [J]. China Foundry, 2012, 9(1): 48−52.

[19] LIU Hong-bao, SHEN Bing, ZHU Ming, ZHOU Xing, MAO Xie-min. Reaction between Ti and boron nitride based investment shell molds used for casting titanium alloys [J]. Rare Metals, 2008, 27: 617−622.

[20] SAHA R L, NANDY T K, MISRA R D K, JACOB K T. Evaluation of the reactivity of titanium with mould materials during casting [J]. Bull Mater Sci, 1989, 12: 481−493.

[21] CHEN Rui-run, DING Hong-sheng, YANG Jie-ren, HUANG Feng, SU Yan-qing, GUO Jing-jie, FU Heng-zhi. Temperature field calculation on cold crucible continuous melting and directional solidifying Ti50Al alloys [J]. Transactions of Nonferrous Metals Society of China, 2012, 22: 647−653.

[22] YANG Jie-ren, CHEN Rui-run, DING Hong-sheng, SU Yan-qing, HUANG Feng, GUO Jing-jie, FU Heng-zhi. Numerical calculation of flow field inside TiAl melt during rectangular cold crucible directional solidification [J]. Transactions of Nonferrous Metals Society of China, 2012, 22: 157−163.

[23] REITZA J, LOCHBICHLERB C, FRIEDRICHA B. Recycling of gamma titanium aluminide scrap from investment casting operations [J]. Intermetallics, 2011, 19: 762−768.

[24] CHASE M W. NIST-JANAF thermochemical tables [M]. 4th ed. Maryland: National Institute of Standards and Technology, 1998.

[25] LIU K, MA Y C, GAO M, RAO G B, LI Y Y, WEI K, WU X H, LORETTO M H. Single step centrifugal casting TiAl automotive valves [J]. Intermetallics, 2005, 13: 925−928.

[26] GAO M, CUI R J, MA L M, ZHANG H R, TANG X X, ZHANG H. Physical erosion of yttria crucibles in Ti−54Al alloy casting process [J]. J Mater Process Technol, 2011, 211: 2004−2011.

[27] LAPIN J, GABALCOVÁ Z, PELACHOVÁ T. Effect of $Y_2O_3$ crucible on contamination of directionally solidified intermetallic Ti−46Al−8Nb alloy [J]. Intermetallics, 2001, 19: 396−403.

[28] CUI R J, TANG X X, GAO M, ZHANG H, GONG S K. Microstructure and composition of cast Ti−47Al−2Cr−2Nb alloys produced by yttria crucibles [J]. Mater Sci Eng A, 2012, 541: 14−21.

[29] TETSUI T, KOBAYASHI T, KISHIMOTO A, HARADA H. Structure optimization of an yttria crucible for melting TiAl alloy [J]. Intermetallics, 2012, 20: 16−23.

[30] CUI Ren-jie, ZHANG Hua-rui, TANG Xiao-xia, MA Li-min, ZHANG Hu, GONG Sheng-kai. Interactions between $\gamma$-TiAl melt

and $Y_2O_3$ ceramic material during directional solidification process [J]. Transactions of Nonferrous Metals Society of China, 2011, 21: 2415−2420.

[31] ZHAO Er-tuan, KONG Fan-tao, CHEN Yu-yong, LI Bao-hui. Interfacial reactions between Ti-1100 alloy and ceramic mould during investment casting [J]. Transactions of Nonferrous Metals Society of China, 2011, 21: s348−s352.

[32] GOMES F, PUGA H, BARBOSA J, RIBEIRO C S. Effect of melting pressure and superheating on chemical composition and contamination of yttria-coated ceramic crucible induction melted titanium alloys [J]. J Mater Sci, 2011, 46: 4922−4936.

[33] CUI R J, GAO M, ZHANG H, GONG S K. Interactions between TiAl alloys and yttria refractory material in casting process [J]. J Mater Process Technol, 2010, 210: 1190−1196.

# Ti-1100 高温钛合金铸造过程中与 CaO 坩埚的界面反应

付彬国，王宏伟，邹鹍鸣，马 盼，魏尊杰

哈尔滨工业大学 金属精密热加工国防科技重点实验室，哈尔滨 150001

**摘 要**：研究了 Ti-1100 高温钛合金和 CaO 坩埚在可控气氛下感应熔炼时的相互作用，并对合金组织、化学成分、显观硬度以及与坩埚的界面反应进行分析。结果表明：合金的铸态组织是典型的魏氏组织。熔融金属和 CaO 坩埚的界面反应是由坩埚轻微的化学溶解和微弱的物理侵蚀引起的。根据线扫描分析，合金在坩埚底部和侧部界面反应区的 $\alpha$ 层厚度分别为 18 和 17 μm，这比采用硬度测试所获得的实验数据要小。$\alpha$ 反应层的形成机制是间隙氧原子。还对 Ti-1100 合金 CaO(s)=Ca+O 反应的标准吉布斯自由能进行了测定，得到 Ca 和 O 的平衡常数和相互作用参数分别为 $\lg K=-3.14$ 和 $e_O^{Ca}=-3.54$。

**关键词**：Ti-1100 合金；CaO 坩埚；界面反应；铸造；组织

**(Edited by Hua YANG)**